Paper No.
2453

Multipronged Characterization of the Corrosion Product Layer Formed on Mild Steel after Exposure to Acetic Acid

Vanessa Fajardo, Bruce Brown, David Young, Srdjan Nešić
Institute for Corrosion and Multiphase Technology
Department of Chemical & Biomolecular Engineering
Ohio University
342 West State St., Athens, OHIO, 45701
United States

ABSTRACT

Organic acids can be present in produced fluids in oil and gas production systems. The most commonly encountered species is acetic acid, which has been hypothesized to damage the protective iron carbonate ($FeCO_3$) layer formed on mild steel in sweet corrosion environments. In laboratory experiments, such an exposure was shown to lead to a temporary increase in the corrosion rate. However, the long term corrosion rate seems to be unaffected [1]. A key objective of this research was to determine how the visually porous $FeCO_3$ layer that survives the attack of acetic acid continues to protect the underlying mild steel. This raises the possibility that there may be a different phase on the steel surface, giving protection, which has been undetected so far. This research sought to identify this phase by characterizing the corrosion product layer using several analytical techniques (SEM, EDS, FIB/TEM/ED, XRD and XPS). This multipronged approach provided a more complete picture of the species found on the steel surface and confirmed that the presence of acetic acid, partially removes the $FeCO_3$ layer. However, the protection is not affected as $FeCO_3$ appears to remain on the surface as a thin surface layer of intergrown nanocrystals

Key words: Iron carbonate, X65 steel, acetic acid, SEM, EDS, FIB/TEM/ED, XRD and XPS.

INTRODUCTION

The formation of iron carbonate, as the main corrosion product on mild steel exposed in CO_2 environments, may retard the corrosion rate, but the presence of acetic acid is thought to damage the $FeCO_3$ layer and temporarily increase the corrosion rate [2]. In spite of acetic acid's effect on the $FeCO_3$ layer, it was found that the long term corrosion rate does not seem to be affected. It remains unclear how the very porous $FeCO_3$ layer that survives the attack of acetic acid continues to protect the underlying steel. This raises the possibility that there may be a different phase on the steel surface, giving protection, which was not detected. This research sought to identify this phase by characterizing the corrosion product layer using different analytical techniques.

EXPERIMENTAL PROCEDURE

A three-electrode setup was used in all the experiments and is shown in Figure 1. X65 mild steel material was used for the rotating cylinder electrode (RCE), which served as the working electrode (WE). A platinum wire was used as a counter electrode (CE) with a saturated silver-silver chloride (Ag/AgCl) reference electrode (RE). The pH was monitored with an electrode immersed in the electrolyte. The temperature was regulated using a thermocouple immersed in the solution and a controller linked to a hot plate.

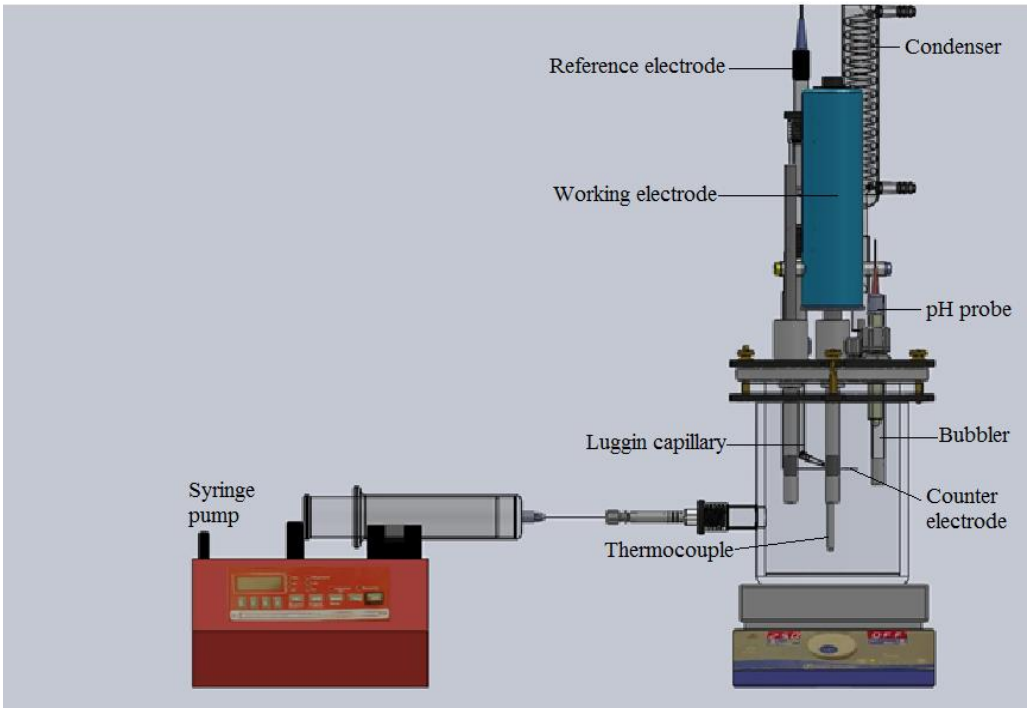

Figure 1: Experimental cell design – $FeCO_3$ layer formation.

The glass cell was filled with 2 liters of electrolyte, which correspond to 1 wt.% NaCl. In all experiments, CO_2 was continuously bubbled through the electrolyte for approximately 1 hour before experimentation and during the entire experimental procedure. This was done in order to ensure that all the dissolved oxygen was removed and to maintain saturation with CO_2 of the test solution. When needed, a hydrochloric acid (HCl) or a sodium bicarbonate ($NaHCO_3$) solution were added to adjust the pH. The experimental temperature was maintained within ±1°C of the desired temperature in all experiments.

To begin each experiment, the steel surface was polished using 240, 320, 400 and 600 grit silicon carbide (SiC) paper sequentially, washed with isopropyl alcohol, dried, mounted on the specimen holder, and immersed into the electrolyte. The open circuit potential was immediately measured. Polarization resistance (Rp) measurements were conducted by polarizing the WE ±5mV from the E_{oc} at a scan rate of 0.1mV/s. The solution resistance was measured independently using alternating current (AC) impedance and the measured Rp was then corrected. AC impedance measurements were done by applying an oscillating potential (±5mV) around the E_{oc} to the WE using the frequency range of 1Hz to 100kHz.

The test matrix used in the $FeCO_3$ precipitation-dissolution experiments is shown in Table 1. The test matrix was carefully selected from a large number of experiments previously done at Ohio University[3]. At the beginning of each experiment, the corrosion rate on the bare steel surface was typically 1 mm/y

and decreased within a few days to values which were approximately one order of magnitude lower (< 0.1 mm/y) as iron carbonate layer formed [3]. The acetic acid was added as a buffered acetic acid solution (to avoid a change in pH) and only after the $FeCO_3$ layer formed.
The corrosion product layer was closely examined using different surface techniques, such as scanning electrode microscopy (SEM), energy-dispersive X-ray spectroscopy (EDS), X-ray photoelectron spectroscopy (XPS), and focused ion beam/transmission electron microscopy/energy-dispersive X-ray spectroscopy (FIB/TEM/EDS).

Table 1
Experimental conditions – $FeCO_3$ precipitation

Test solution	Deionized water + 1 wt.% NaCl
Test material	API X65 steel
Temperature	80°C
Total pressure of CO_2	0.53 bar
Undissociated (free) organic acid	3 mM
pH	6.3
Rotation velocity	Stagnant conditions
Initial supersaturation	200
Sweep rate	0.1 mV/s to 0.2 mV/s
Polarization resistance	From -5mV to 5mV (vs E_{oc})
AC Impedance	± 5mV *vs.* E_{oc} from 1mHz to 100KHz

RESULTS

A detailed surface analysis approach was needed in order to determine the nature of the thin corrosion product layer remaining after the action of the acetic acid. The first step was carried out using SEM and EDS to provide the morphology and the elemental analysis of the corrosion product layer formed on the steel surface before and after acetic acid was added to the bulk solution. The SEM showed a partial removal of the $FeCO_3$ (Figure 2). The EDS analysis of the exposed substrate showed lower intensity peaks of Fe, O and C, constituent elements that form $FeCO_3$, compared with the EDS done on the prismatic crystals (Figure 2). However, this elemental analysis is inconclusive since it is not possible to identify the exact chemical composition of the compound. It is easy to misinterpret the results based only on the ratios of atomic weight percent provided by EDS.

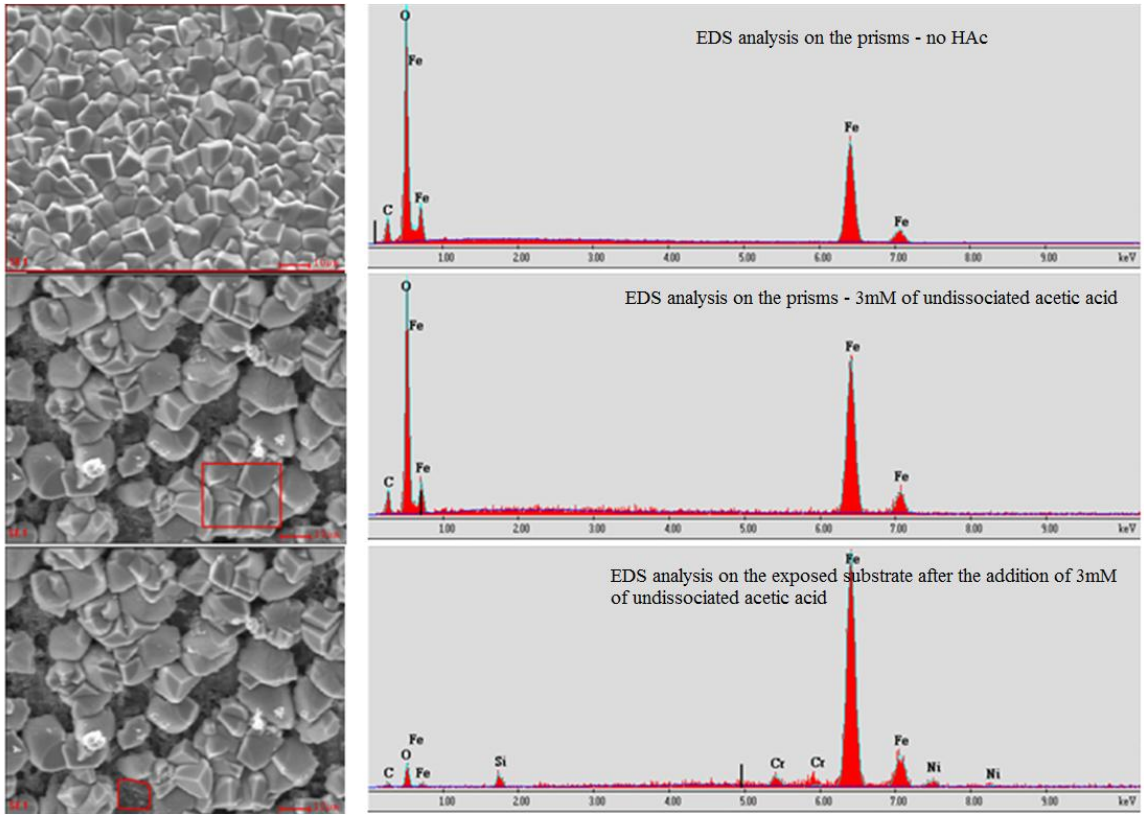

Figure 2: EDX analysis before and after the addition of 3mM of undissociated acetic acid (X65 steel substrate, stagnant conditions and 80°C).

Based on the known aqueous chemistry in these experiments, it could be possible to have cementite (Fe_3C), siderite ($FeCO_3$), hematite (Fe_2O_3), magnetite (Fe_3O_4) and various forms of iron hydroxide, on the steel surface. In order to distinguish between these possible compounds, additional analyses had to be conducted. Using transmission electron microscopy (TEM) it is possible to obtain electron diffraction (ED) data. The generated diffraction pattern is unique to the crystal structure of the compound or element present in characterized solid phases and depends solely on the geometry and symmetry of the unit cell[4,5]. Small areas can be selected for acquisition of diffraction data down to a length scale of 300nm. The rings obtained from the diffraction data provide the d-spacings for each unique phase: pure element or compound. For the purpose of this study, it is important to determine the crystal structure of the thin layer formed on the steel, since hematite and siderite share the same hexagonal unit cell type and have certain similarities in their diffraction patterns as shown in Figure 3. As magnetite is a cubic structure, as shown in Figure 3, it will be easy to distinguish from other possible phases if it is present in the system.

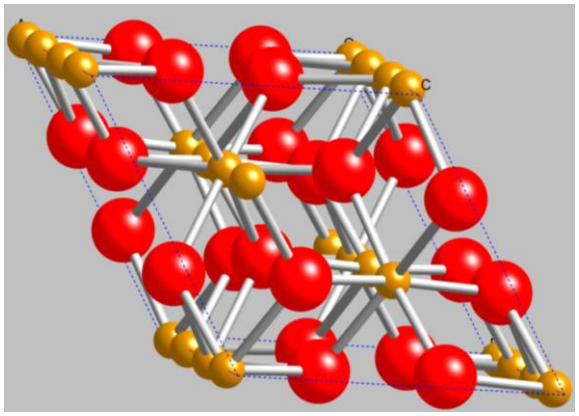

Hematite (Fe_2O_3)
Hexagonal crystal system
a: 5.038Å, c: 13.772Å [6]

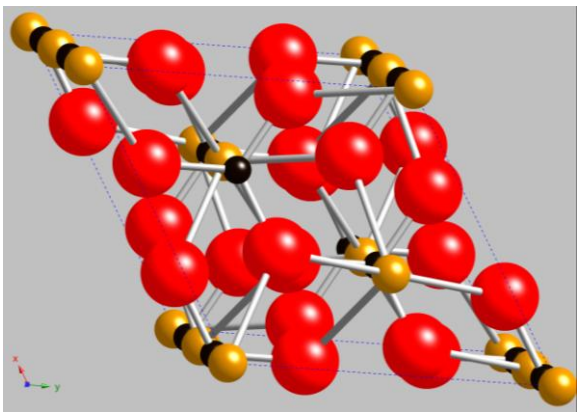

Siderite ($FeCO_3$)
Hexagonal crystal system
a: 4.694Å, c: 15.386Å [7]

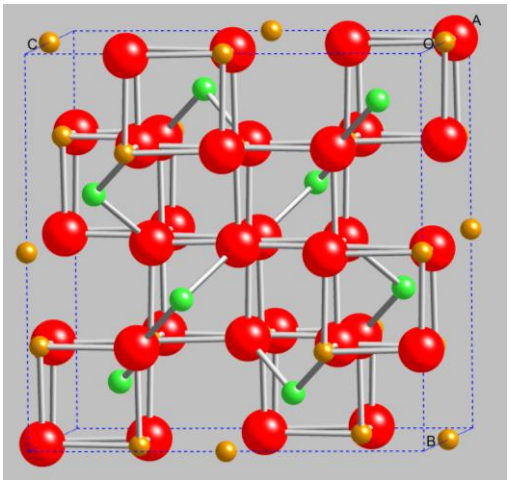

Magnetite[(1)] (Fe_3O_4)
Cubic crystal system
a: 8.396Å [8]

Figure 3: Unit cells of hematite, siderite and magnetite [(2)] (a and c= unit cell edges).

Diffraction data from the International Center for Diffraction Data[(3)] (ICDD) show that the highest intensity peaks for hematite and siderite are found very close to each other with d-spacings of 2.703 and 2.795Å, respectively, as shown in Figure 4 and Table 2.

[(1)] This is a spinel-type ($MgAl_2O_4$) structure with Fe^{2+} and Fe^{3+} occupying different positions within the lattice, in analogy to Mg^{2+} and Al^{3+}

[(2)] Sofware used: CrystalMaker

[(3)] International Center for Diffraction Data (ICDD), 12 Campus Blvd., Newtown Square, PA 19073-3273

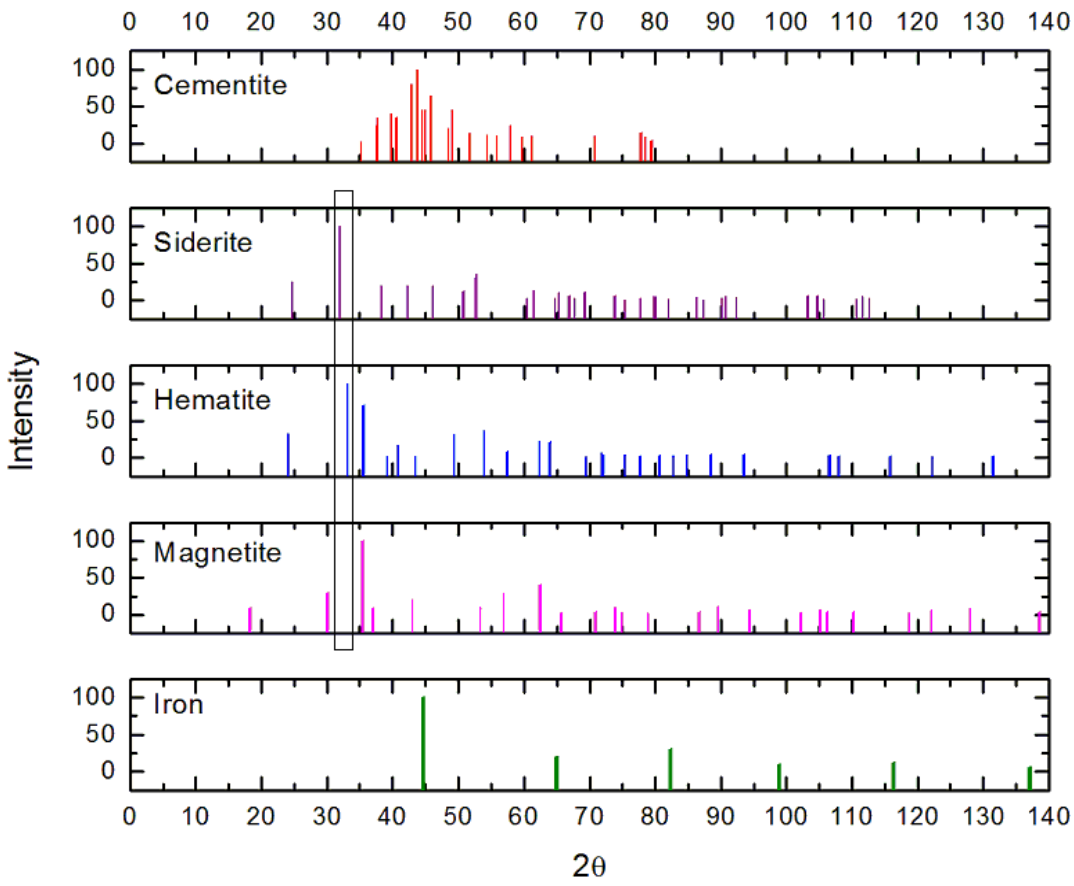

Figure 4: XRD analysis of possible compounds founds on the steel surface with λ= 1.54056 Å (Source: ©2010 International Centre for Diffraction Data).

Table 2
d–Spacings with $\lambda = 1.54056(\text{Å})$ [4]

Iron		Magnetite		Hematite		Siderite		Cementite	
$d(\text{Å})$	Intensity	$d(\text{Å})$	Intensity	$d(\text{Å})$	Intensity	$d(\text{Å})$	Intensity	$d(\text{Å})$	Intensity
2.027	100	4.852	8	3.686	33	3.593	25	2.547	2
1.433	20	2.967	30	2.703	100	2.795	100	2.387	25
1.170	30	2.532	100	2.519	70	2.564	<1	2.381	35
1.013	10	2.424	8	2.295	2	2.346	20	2.264	40
0.906	12	2.099	20	2.208	17	2.134	20	2.219	35
0.828	6	1.715	10	2.080	2	1.965	20	2.108	80
		1.616	30	1.843	31	1.797	12	2.068	100
		1.485	40	1.697	36	1.738	30	2.032	45
		1.419	2	1.601	8	1.732	35	2.014	45
		1.328	4	1.601	8	1.529	3	1.978	65
		1.281	10	1.487	22	1.506	14	1.873	20
		1.266	4	1.454	21	1.439	3	1.854	45
		1.212	2	1.351	2	1.427	11	1.764	14
		1.122	4	1.313	7	1.397	6	1.685	12
		1.093	12	1.308	4	1.382	3	1.685	12
		1.050	6	1.260	4	1.355	11	1.642	10
		0.990	2	1.229	2	1.282	5	1.590	25
		0.970	6	1.191	3	1.259	1	1.547	8
		0.963	4	1.191	3	1.227	3	1.512	10
		0.939	4	1.165	3	1.200	5	1.330	10
		0.895	2	1.142	4	1.198	4	1.330	10
		0.880	6	1.104	4	1.174	2	1.226	14
		0.857	8	1.057	4	1.125	4	1.217	8
		0.823	4	0.961	3	1.115	1	1.205	4
		0.812	6	0.960	3	1.087	3		
		0.808	4	0.952	2	1.082	5		
				0.909	2	1.067	4		
				0.879	2	0.983	5		
				0.845	2	0.972	5		
				0.845	2	0.967	2		
						0.936	2		
						0.931	6		
						0.926	3		

Thus, it is clear that a single analytical technique such as EDS does not provide enough information about any compound formed on the surface for adequate identification. The electron diffraction data in conjunction with the XRD provide the best accuracy for the detection and identification of compounds in local areas on sample surfaces. The positions and intensities of an element's or a compound's XRD

[4] For conversion to 2θ angle, Braggs law should be applied (n λ=2d sin θ)

peaks or ED spots from an analyzed crystal are related to reflections from the lattice planes encountered [4] as shown in Figure 5.

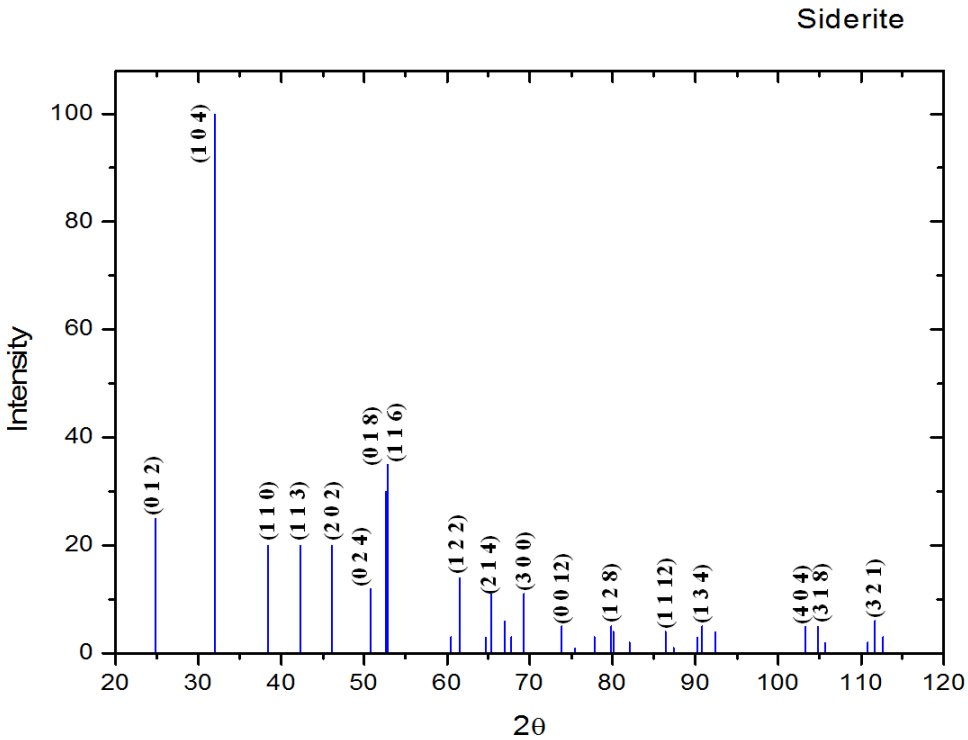

Figure 5: XRD analysis of $FeCO_3$ (Source: ©2010 International Centre for Diffraction Data).

To relate the XRD data with the electron diffraction pattern it is necessary to conduct FIB/TEM analyses of the samples. The focused ion beam (FIB) mills the sample to a scale of nanometers, as shown in Figure 6. Then, the transmission electron microscopy (TEM) provides an image of the crystal structure down to the crystal lattice, providing the diffraction data.

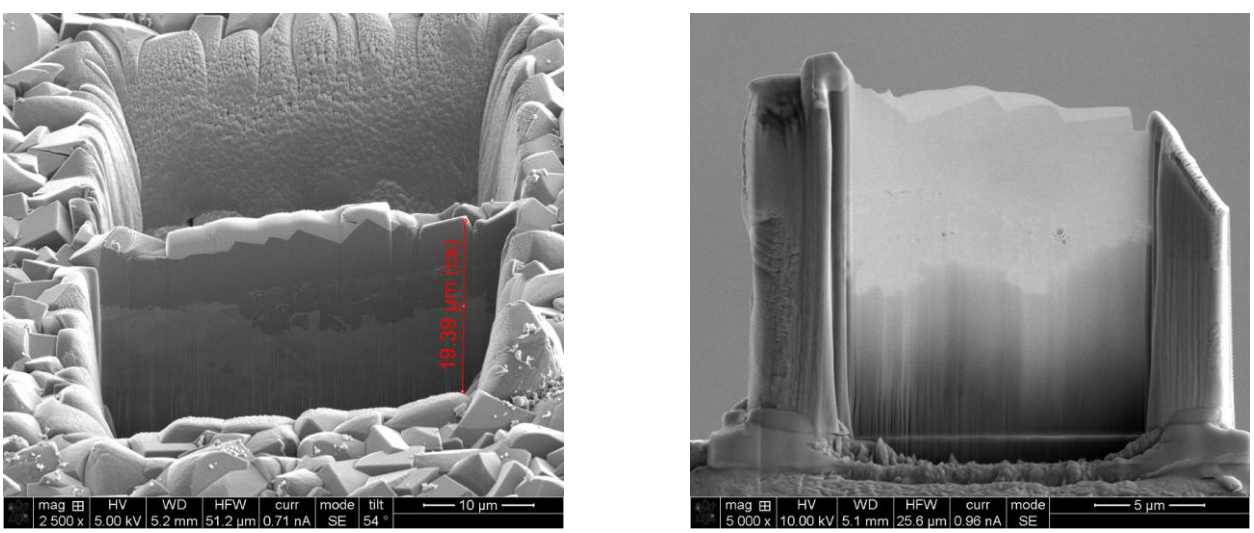

Figure 6: FIB images of $FeCO_3$ plates formed on X65 mild steel.

The samples were analyzed using TEM/EDS techniques after the precipitation of $FeCO_3$ (before the acetic acid was added) and after the dissolution processes induced by the addition of the acid. In the precipitation process, both plates and prisms of $FeCO_3$ formed. Even though the morphology of the precipitates is different, the TEM/EDS showed that both were $FeCO_3$ (Figure 7 and Figure 9:). Electron diffraction data confirmed this assumption (Figure 8 and Figure 10). The Bragg reflections (interplanar spacing d_{hkl}) obtained from the lattice planes for the plates are: R_1[1 1 2], R_2[1 0 4], R_3[1 1 0] and R_4 [0 1 2], which correspond to some of the major peak intensities of $FeCO_3$, according to XRD data from the ICDD. Every d-spacing has a corresponding XRD 2θ value and *hkl* planes (Figure 5), which further confirms the type of compound present on the surface. For every electron diffraction pattern, d-spacing was calculated using $\lambda L = 1.935 \mathring{A} cm$.

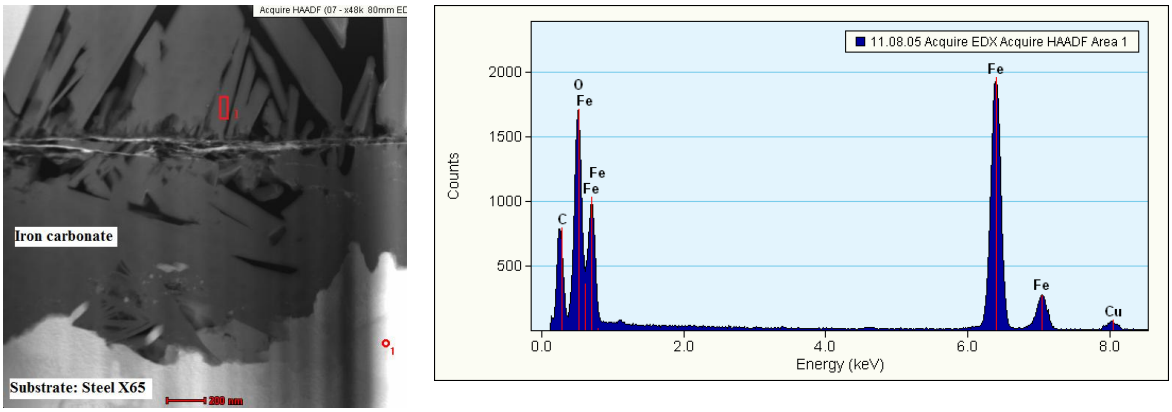

Figure 7: TEM image and EDS analysis of $FeCO_3$ plates formed on X65 mild steel.

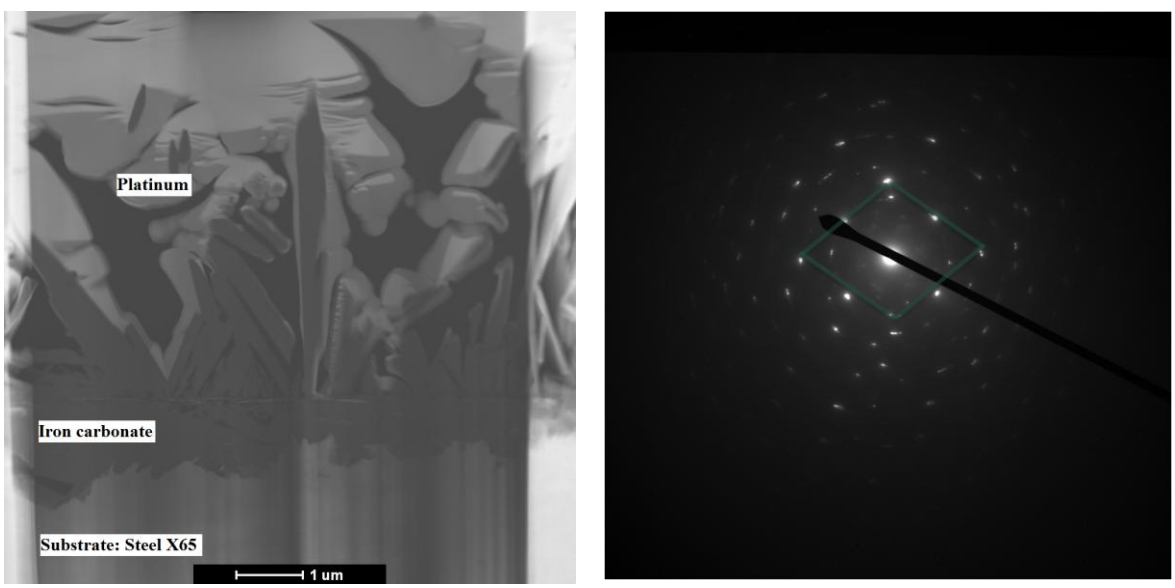

Figure 8: TEM image and ED data of the plates found on the X65 mild steel before the addition of undissociated acetic acid.

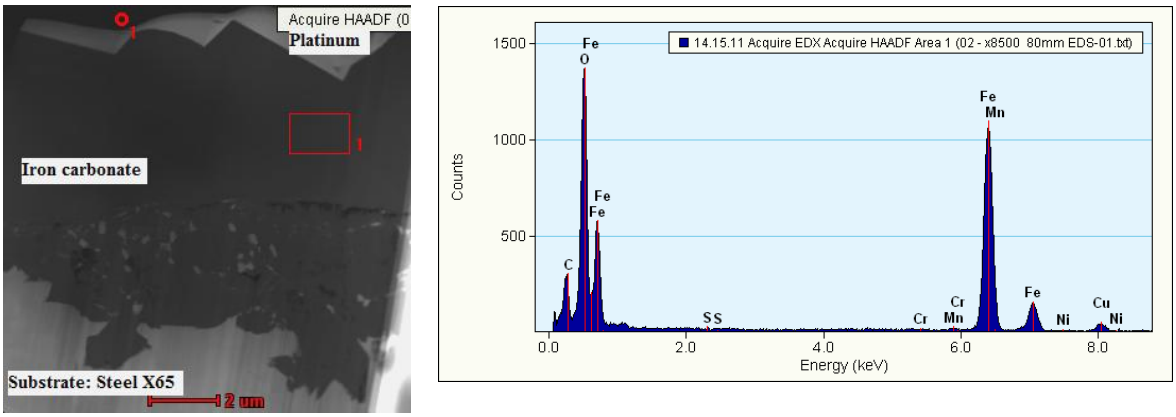

Figure 9: TEM image and EDS analysis of $FeCO_3$ prisms formed on X65 mild steel.

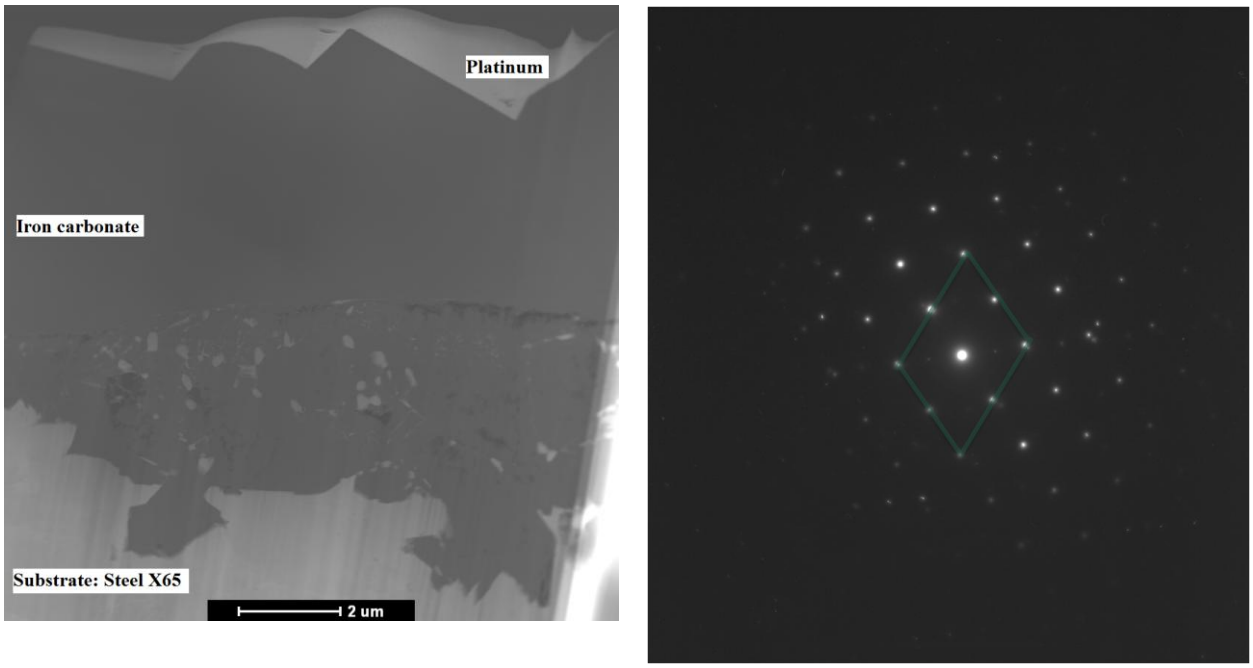

Figure 10: TEM image and ED data of the prisms found on the X65 mild steel before the addition of undissociated acetic acid.

After the dissolution process by the addition of acetic acid, only prisms of $FeCO_3$ remained on the steel surface. The electron diffraction patterns of the prisms found on the steel showed a hexagonal geometry. The d-spacings corresponded to those of siderite (Figure 11:). Although the morphology of the exposed substrate looks amorphous, it is possible that the scale remaining on the steel surface is an agglomeration of nanocrystals. This may be explained by the electron diffraction pattern for the powder formed in the bulk solution as shown in Figure 12. The sizes of the intergrown nanocrystals are of the order of ~58nm (0.05μm). Agglomeration of such nanocrystals may resemble an amorphous phase when observed at higher magnifications. The ED data is consistent with $FeCO_3$.

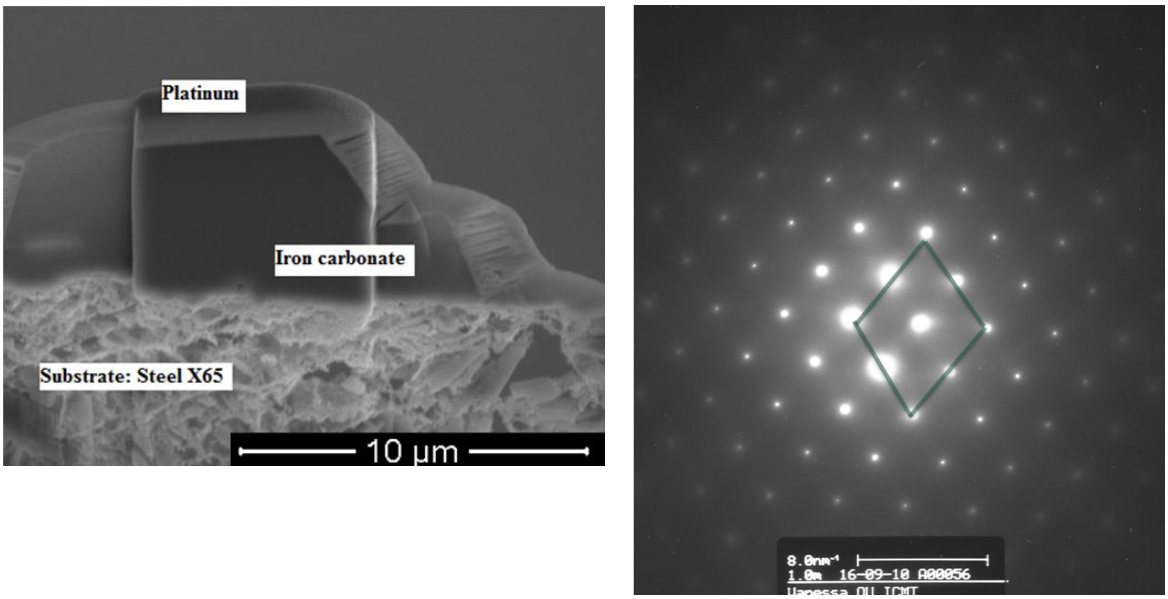

Figure 11: TEM image and ED data of the prism found on the X65 mild steel after the addition of undissociated acetic acid.

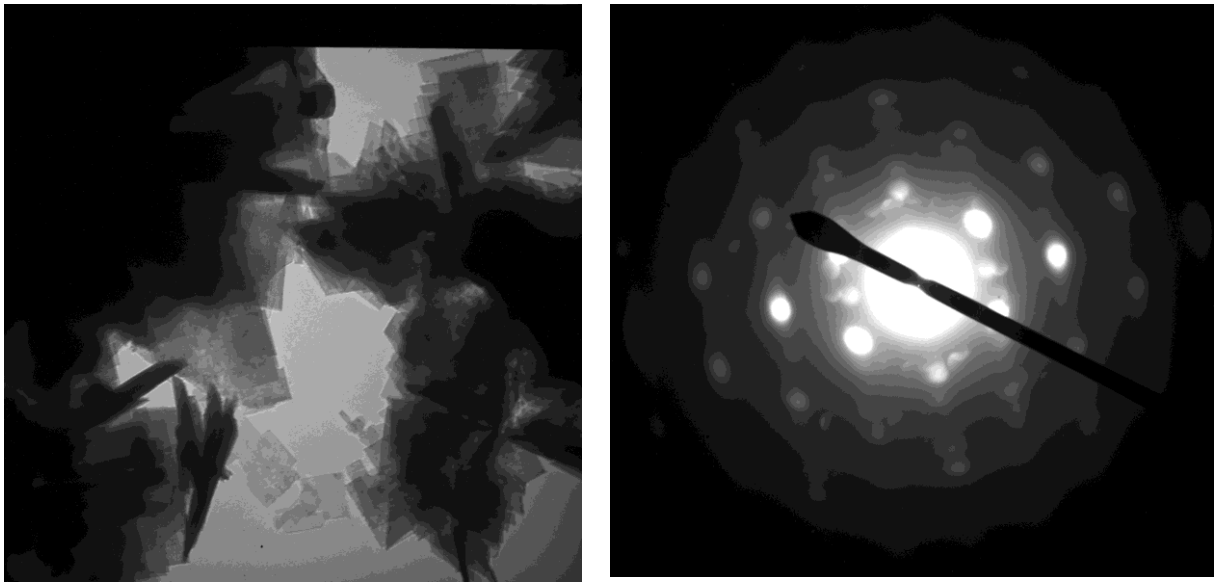

Figure 12: $FeCO_3$ nanocrystals and ED data.

In addition, XPS was utilized to confirm the results obtained by the other techniques. Figure 13 shows the XPS scans of the $FeCO_3$ scale formed on X65 steel which matches the theoretical binding energy for $FeCO_3$ [9].

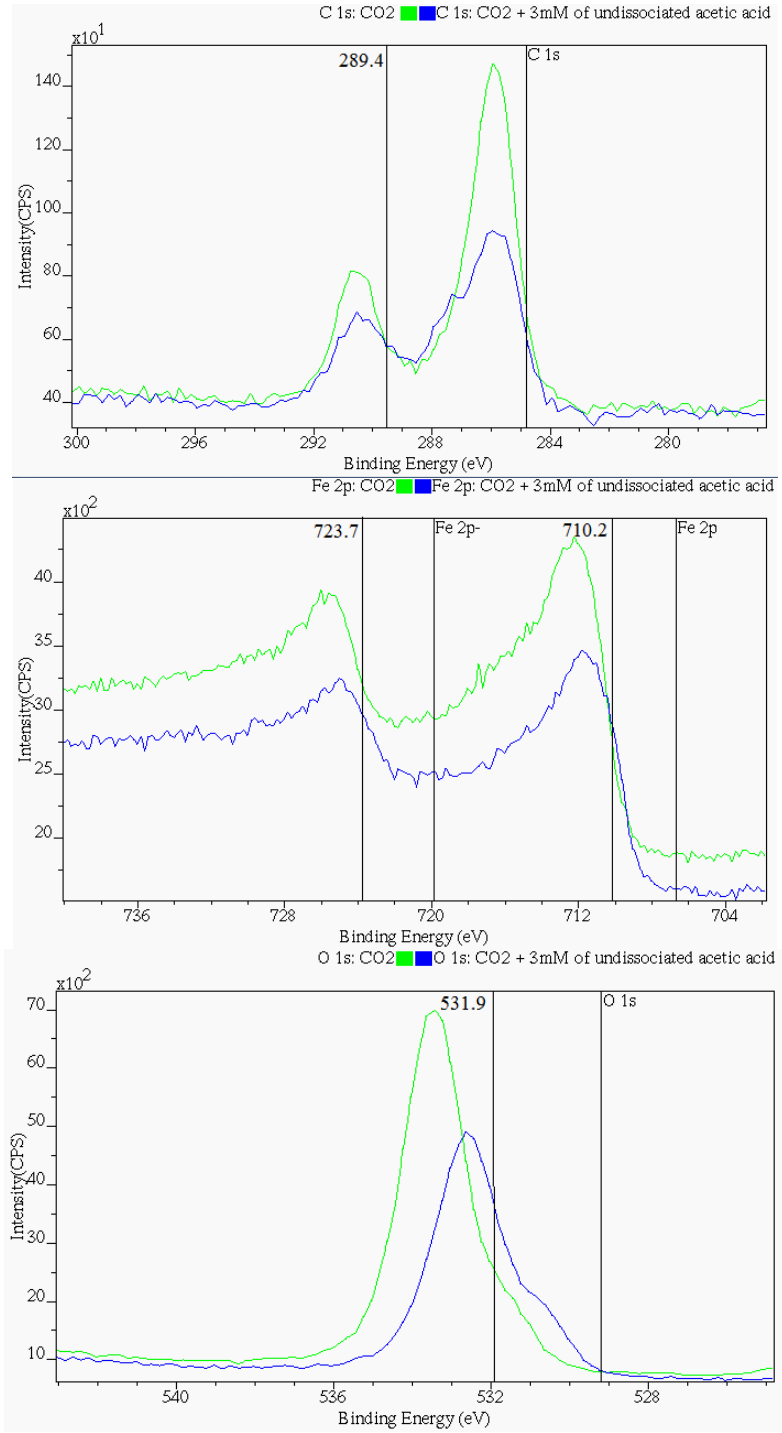

Figure 13. XPS scans of $FeCO_3$ dissolution on X65 steel in the presence of acetic acid (80°C, 0.1wt.% NaCl, and pCO_2=0.53 bar).

CONCLUSIONS

The presence of acetic acid, at a constant pH, partially removed the $FeCO_3$ layer. However, the protection stayed, because part of the $FeCO_3$ remained on the surface. This $FeCO_3$ is a very thin surface layer of intergrown $FeCO_3$ nanocrystals. Several surface analyses methods have proven this hypothesis (SEM, EDS, XRD, XPS, FIB/TEM/EDS and ED data).

ACKNOWLEDGEMENTS

The different surface analysis techniques were done in the Department of Physics and Astronomy at Ohio University under the supervision and guidance of Dr. Ingram, Dr. Martin Kordesch and Dr. Aurangzeb Khan. The Department of Materials Science and Engineering in CASE Western Reserve University, under Dr. Amir Avishai's supervision, was also instrumental in allowing me to complete this project. In particular, Dr. Kordesch provided me with valuable feedback on the diffraction data analysis.

REFERENCES

1. Fajardo, V., Canto, C., Brown, B., and Nesic, S., "The Effect of Acetic Acid on the Integrity of Protective Iron Carbonate Layers in CO_2 Corrosion of Mild Steel."CORROSION/08, paper no.08333. Houston, TX:NACE, 2008.

2. Gulbrandsen, E., "Acetic Acid and Carbon Dioxide Corrosion of Carbon Steel Covered with Iron Carbonate."CORROSION/07, paper no.7322. Houston, TX:NACE, 2007.

3. Fajardo, V. "Localized CO_2 Corrosion in the Presence of Organic Acids."Master of Science, Ohio University,2011.

4. Bloss, D.F. *Crystallography and Crystal Chemistry an Introduction.* 1st edition. United States: Holt, Rinehart and Winston, Inc, 1971, pp. 545.

5. West, A.R. *Solid State Chemistry and its Applications.* 10th edition. Great Britain: John Wiley & Sons, 1998, pp. 734.

6. Blake, R., Hessevick, E., Zoltai, T., "Refinement of the Hematite Structure." The American Mineralodist 51, (1966): p. 123-129.

7. Graf, L. D."Crystallographic Tables for the Rhombohedral Carbonates." The American Mineralodist 46, 1283(1961): p. 1313.

8. Wechsler, B. A., Lindsley, D. H., and Prewitt, C. T., "Crystal Structure and Cation Distribution in Titanomagnetites ($Fe_{3-x}Ti_xO_4$)." American Mineralogist 69, (1984): p. 754-770.

9. Heuer, J. K., and Stubbins, J. F., "An XPS Characterization of $FeCO_3$ Films from CO_2 Corrosion." Corrosion Science 41, 7(1999): p. 1231-1243.